

High-temperature magnetic and optical properties of CdTe-MnTe superlattices

P. Kossacki, Nguyen The Khoi, and J. A. Gaj

Institute of Experimental Physics, Warsaw University, Hoża 69, 00-681 Warsaw, Poland

G. Karczewski, J. Kossut, and T. Wojtowicz

Institute of Physics, Polish Academy of Sciences, aleja Lotników 32/46, 02-668, Warsaw, Poland

(Received 16 July 1998; revised manuscript received 4 November 1998)

We present a study of magnetic and magneto-optical properties of $\text{Cd}_x\text{Te}_{1-x}$ -MnTe superlattices up to the room temperature. A comparison of low-temperature exciton Zeeman effect and the measurements of the magnetization performed by superconducting quantum interface device magnetometer shows a perfect agreement with a model description, thus allowing for determination of Mn content profiles width throughout the structures. Precise high-temperature Zeeman effect measurements show that the exciton splitting decreases with temperature faster than expected on the basis of the Curie-Weiss law. We attribute this effect to the influence of thermal fluctuations on exciton states. [S0163-1829(99)05311-4]

I. INTRODUCTION

Cadmium manganese telluride is one of the best-known semimagnetic (diluted magnetic) semiconductors. Their introduction in quantum semiconductor structures has added a new dimension to the band-gap engineering allowing to tailor these structures not only by controlling the growth processes but also by varying the energies using an external magnetic field.¹ The introduction of magnetic ions has brought a variety of effects related to ion-carrier interactions specific for heterostructures with diluted magnetic semiconductors such as spin superlattices,^{2,3} magnetic field-induced type I–type II transition,⁴ observation of above-barrier states,⁵ free-magnetic polaron formation,^{6,7} ferromagnetic phase,⁸ or variation of relative valence-band offsets with temperature.⁹

Studies of excitonic Zeeman effect in $\text{CdTe}/\text{Cd}_{1-x}\text{Mn}_x\text{Te}$ quantum wells and superlattices have also helped to understand the role of interface mixing and allowed to create a magneto-optical method of interface characterization.^{10,11} The method makes use of numerical simulations of the respective quantum well potentials for electrons and holes with interfaces assumed to be not abrupt, but containing regions of diluted barrier material. The dilution decreases the influence of ion-ion interaction, which favors an antiparallel alignment of Mn^{++} spins at low temperatures. Therefore, interface mixing results in an enhancement of the magnetization in regions penetrated by excitons, and thus it leads to a strong increase of excitonic Zeeman splitting. The enhancement makes the Zeeman effect very sensitive to the interface mixing in $\text{CdTe}/\text{Cd}_{1-x}\text{Mn}_x\text{Te}$ system (see, for example, Refs. 12–14), especially for high-Mn concentrations in the barriers where the magnetization is strongly suppressed by antiferromagnetic ion-ion exchange interaction.

In the region of low temperatures there is no theoretical simulation correctly reproducing the magnetization of bulk $\text{Cd}_{1-x}\text{Mn}_x\text{Te}$ in a wide range of magnetic ion concentrations. Such a description exists only in the low-concentration limit.¹⁵ An empirical formula for low-temperature bulk magnetization¹⁰ is commonly used in model calculations.

The magnetic properties near the interface are not well known and, therefore, any model calculation requires some important but not well-grounded assumptions.

Two effects influence the magnetization at the interface: an intrinsic effect due to magnetic properties of the interface itself, and an extrinsic one due to dilution of the interface material.¹⁰ Both effects play a similar role in the enhancement of the Zeeman splitting and it is very difficult to distinguish experimentally one from another on the basis of low-temperature data. Therefore, the relative role of both contributions has been subject to many controversies. Several different competitive models have been proposed.^{10,16} Such assumptions are no longer necessary if the temperature is high enough to make the high-temperature expansion approach to the magnetization or susceptibility valid. In such case an accurate calculation of the interface magnetization is possible.

In the present paper, we perform a simultaneous analysis of low-temperature Zeeman data and high-temperature measurements of both magnetization and the Zeeman splitting of exciton. Precise superconducting quantum interface device (SQUID) measurements of very thick superlattices allowed us to test magnetic properties of the interface regions. We also utilize the high-temperature approximation to analyze magneto-optic data. The presence of clearly visible reflectivity structures up to temperatures as high as the room temperature allowed us to measure the Zeeman effect in the temperature range not accessible for magneto-optical experiments in bulk crystals.

II. SAMPLES AND EXPERIMENT

We studied structures grown by molecular-beam epitaxy (MBE) from CdTe, Te, Cd, and Mn sources on (100)-oriented GaAs substrates with thick CdTe buffers. The substrate temperature during the growth was approximately 240 °C.

The superlattice samples (SL 09124, SL 09094, and SL 09074) contained 200 periods of CdTe wells separated by MnTe barriers of the thickness 2, 4, and 8 monolayers, re-

spectively. The thickness of the wells was equal to 40 Å.

The above parameters were chosen to assure good sensitivity of both magnetic and magneto-optic measurements. The large number of superlattice period repetitions was necessary to obtain a measurable magnetization contribution related to the interfaces. In order to maximize the relative contribution of interfaces we used thin barrier layers. Also we polished off the substrates and used samples without $\text{Cd}_{1-x}\text{Mn}_x\text{Te}$ buffer layers (which sometimes are preferable to CdTe buffers in structures used for magneto-optical experiments). The use of superlattices (rather than single quantum wells) assured also sufficient exciton oscillator strength, making the reflectivity features easily discernible even at high temperatures.

The barrier Mn mole fraction was nominally 100%. At such concentration the magnetization is strongly suppressed by the ion-ion antiferromagnetic interaction even at high temperature, making the relative contribution of the diluted interface regions quite important. The well width was chosen to be sufficiently small, to assure sufficient penetration of excitonic wave functions into the barriers, and thus to obtain an easily measurable Zeeman effect.

Magnetization was measured by a SQUID magnetometer at temperature ranging from 10 to 300 K. The magnetic field was parallel to the sample surface and ranged up to 1 T. Before measurement the sample substrate was polished off mechanically down to about 140 μm . The samples, of the area of at least 2 cm^2 , were cut into pieces $3 \times 3 \text{ mm}^2$ and glued together in a stack. Such samples were mounted in a thin plastic straw by a General Electric varnish.

All magnetorefectivity measurements were performed in the Faraday configuration with magnetic field perpendicular to the sample surface. The samples were mounted strain-free in a superconducting magnet and immersed in superfluid helium at 1.9 K. The higher temperature reflectivity measurements were performed in the same setup with samples in gaseous helium under atmospheric pressure. In order to obtain a high accuracy of the exciton splitting at high temperatures a polarization modulation technique was applied, similar to that used by Coquillat *et al.*¹⁷ Photoluminescence was excited with an Argon-ion laser providing 2–40 mW over a spot of diameter between 0.1 and 1 mm. Optical measurements were done with use of Oriel Instaspec IV CCD detector.

III. LOW-TEMPERATURE ZEEMAN CHARACTERIZATION

The low-temperature reflectivity spectra, obtained on one of the superlattices in several fields up to 5 T are shown in Fig. 1. The features in two circular polarizations related to the creation of the heavy-hole exciton ground states at 5 T are marked by vertical lines. The reflectivity feature is broader than exciton lines measured for typical single quantum wells due to, possibly, variation of the well thickness. The horizontal line in Fig. 1 represents the change of the exciton energy due to a one monolayer change of the well width. In the case of our relatively thick structures with 200 periods, the linewidth comparable to a variation of the quantum well width by only one monolayer points to a good overall quality of the structure. We used a simple way of

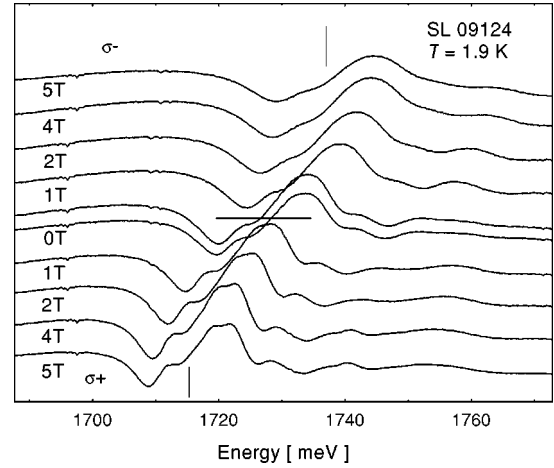


FIG. 1. Low-temperature reflectivity spectra in magnetic field for superlattice SL 09124.

pointing the energy of the reflectivity structures at halfway between their maximum and minimum. It is known that, depending on light interference effects in the sample, the form of the reflectivity structures may be very different and a precise determination of transition energy requires a suitable model description of the spectra.¹⁸ However, the broadening mechanism possible in our superlattices (lack of perfect stability of the growth parameters leading to a variation of the well thickness) is rather difficult to model. On the other hand we use splitting values rather than absolute energy values, therefore our results are reasonably insensitive to the method of pointing of energies.

Low-temperature Zeeman splitting was used for precise characterization of the superlattices. The exciton splitting was interpreted in terms of the model described in Ref. 10. We assumed an intermixing profile between CdTe and $\text{Cd}_{1-x}\text{Mn}_x\text{Te}$ represented by an exponential function, with a characteristic length l_{int} .

Such a profile is expected for a segregation mechanism, i.e., an exchange of atoms between neighbor layers during the growth.¹¹ It gives a strongly asymmetric Mn distribution in the well, with a tail extending into the well only from the barrier, which was grown first. Variations of the potential in the plane of the interface were neglected. The potential profiles across the interfaces were calculated using bulk magnetization dependence for local Mn mole fraction. The intrinsic enhancement of a low-temperature interface magnetization was included as in Ref. 10, by introduction of an effective Mn concentration x_{eff} as a function of distance in the direction perpendicular to the interface

$$x_{\text{eff}} = \frac{x(z-d) + x(z) + x(z+d)}{3}, \quad (1)$$

where d is a monolayer thickness. The local magnetization M_{loc} is obtained from the dependence $M(x)$ in the bulk

$$M_{\text{loc}}(z) = \frac{M[x_{\text{eff}}(z)]}{x_{\text{eff}}(z)} x(z). \quad (2)$$

The ground states of electrons and heavy holes were found by numerical integration of the one-dimensional Schrödinger equation as a function of the magnetic field.

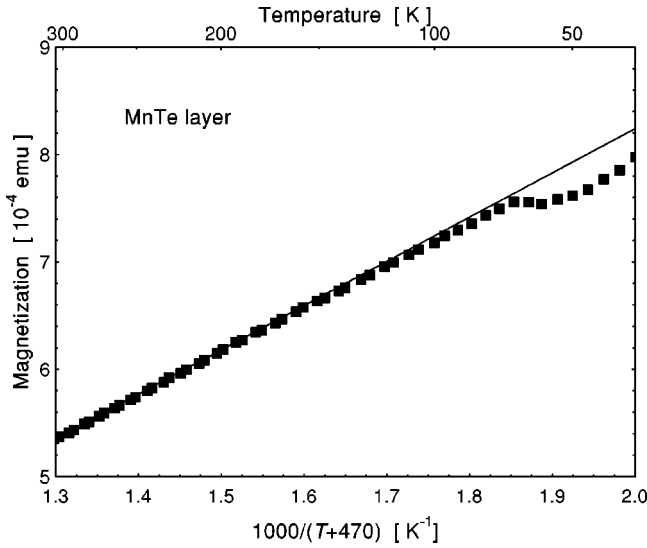


FIG. 2. Magnetization of 4.5- μm thick MnTe layer versus temperature. Line represents Curie-Weiss law with coefficients extrapolated from lower concentrations.

Transition energies were obtained for the two circular polarizations with the exciton binding energies taken independent of the magnetic field and equal to the values obtained for similar quantum wells. The intermixing length and well thickness were determined by fitting the calculated spin-split exciton energy to the experimental data. The intermixing length was obtained to be 4.65, 4.67, and 4.88 \AA for the superlattices with barriers of 2, 4, and 8 monolayers, respectively. This means that the Mn concentration in the well decreases from 100% at the end of the barrier to about 1% at the center of the well and to about 0.02% directly before the beginning of the next barrier. The obtained intermixing length values are typical for the MBE-grown superlattices. We must stress here that in spite of a relatively long growth time of our superlattices the intermixing length is of the same order as the values reported for much thinner structures, such as single quantum wells. This fact supplies an additional argument for the segregation intermixing mechanism, as opposed to the diffusion one. Let us also note that intermixing values are mostly sensitive to the Zeeman splitting and much less to zero-field exciton energy. Therefore any inaccuracy in the assignment of a particular point on the reflectivity structure to the exciton line, as well as inaccuracy of exciton binding energy have minor influence on the results of the present paper.

IV. MAGNETIZATION AT HIGH TEMPERATURE

The magnetization was analyzed in the temperature range for which the susceptibility of $\text{Cd}_{1-x}\text{Mn}_x\text{Te}$ obeys the Curie-Weiss law.^{19,20} It is well known that, for low concentrations of Mn ions, the law is followed with high accuracy, but for high concentrations there are no accurate experimental data available. Since the superlattices used by us contained material with Mn content varying from 0 up to 100%, we decided to check experimentally the accuracy and the applicability range of the Curie-Weiss law. A sample containing a 4.5- μm thick MnTe layer had been measured by SQUID. The susceptibility versus temperature is presented in Fig. 2. The

solid line represents susceptibility obtained for the Curie-Weiss temperature and Curie constant (assuming $S=5/2$) extrapolated from the bulk samples with lower Mn content²⁰ ($\Theta = \vartheta x$, and $\vartheta = -470$ K). It is clear that for temperatures above 100 K, the high-temperature expansion is applicable.

That result allows us to use this simple approximation for the calculation of the magnetization of the superlattices. In our simulations the local magnetization was obtained as a function of the distance z in the direction perpendicular to the interface

$$M(z) = \frac{C(z)B}{T - \Theta(z)}. \quad (3)$$

$C(z)$ is the Curie constant proportional to the Mn content $x(z)$

$$C(z) = N_0 (g \mu_B)^2 S(S+1) x(z) / (3k_B). \quad (4)$$

N_0 denotes the number of cation sites per unit volume, μ_B is the Bohr magneton, k_B the Boltzmann constant, and g and S stand for the Landé factor and the spin of the Mn ion, respectively. The Curie-Weiss temperature Θ depends on the ion-ion exchange interaction constant and may be expressed by

$$\Theta(z) = \frac{2}{3} S(S+1) \sum_n \zeta_n J, \quad (5)$$

where ζ_n denotes the average number of Mn neighbors of an ion at a particular position in the structure and J the Heisenberg-like exchange constant. Such approach describes both “intrinsic” and “extrinsic” interface effects and is accurate within the high-temperature expansion. In our simulations we have taken into account only the nearest magnetic neighbors with the exchange integral $J = -6.7$ K.²⁰ This parameter describes well the Curie-Weiss behavior of the bulk $\text{Cd}_{1-x}\text{Mn}_x\text{Te}$. We checked that including interactions between more distant neighbors did not change the results appreciably.

The experimental data obtained for superlattices is presented in Fig. 3. One can note that the magnetization decreases almost linearly versus logarithm of the temperature. A simple calculation (see Appendix) shows that, approximately, such a dependence is expected for an exponential decay of Mn concentration at MnTe \rightarrow CdTe interface. A leading role of such a dependence provides an additional argument for an importance of interface contribution to the magnetization. Due to the dilution at the interface, the contribution of an interface ion to the magnetization may exceed by orders of magnitude that of the ions lying deep in the barrier.

Since the absolute value of the magnetic susceptibility of a sample contains some uncertainty due to the glue used for mounting it, only the slope of the temperature variation was analyzed. It was checked by a separate measurement on bare substrates prepared identically as the samples with superlattices that the magnetization of the glued substrates does not vary in the experiment’s temperature range. A simple dependence $\alpha + \beta \times \ln(T)$ was fitted to the experiment and then the coefficient β was compared to the results of the fitting of the same function to the numerical simulations with different

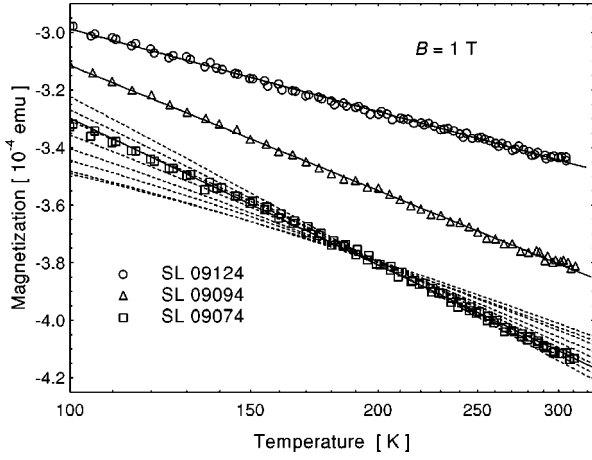


FIG. 3. Magnetization of superlattices versus temperature (in logarithmic scale). The data have been shifted vertically in order to fit on one figure samples with different amount of diamagnetic substrate (GaAs). The dotted lines represent simulations with intermixing parameter equal to 0, 1, 2, 3, 4, 5, 6, and 7 Å. The solid lines represent fits of function $\alpha + \beta \times \ln(T)$.

intermixing length l_{int} . The results of both fits obtained from SQUID and low-temperature magneto-optic measurements are combined in Table I. For all samples the experimental data obtained from both methods and results of simulations (with exponential profile EXP) are in a very good agreement.

The SQUID data are not sensitive to any exciton effects, and are compared to the exact high-temperature simulation. Thus a comparison of the high-temperature magnetization and low-temperature Zeeman effect allows to test directly the hypothesis concerning the importance of both ‘‘intrinsic’’ and ‘‘extrinsic’’ contributions introduced in the analysis of low-temperature data. To test the sensitivity of our analysis to the choice of the interface profile we repeated simulations for several profiles. In particular, the results obtained with the use of the error function¹⁰ (ERF) are presented in Table I. The intermixing length necessary to recover the observed Zeeman splitting gives slightly larger magnetization slope (β) than the experimental values, however it remains within experimental accuracy. The other profiles tested by us were abrupt profiles (STEP), for which the intermixing appears only between two monolayers closest to the interface.¹⁶ The percentage of ions mixed between the monolayers is given by parameter χ . A perfect abrupt interface is represented by

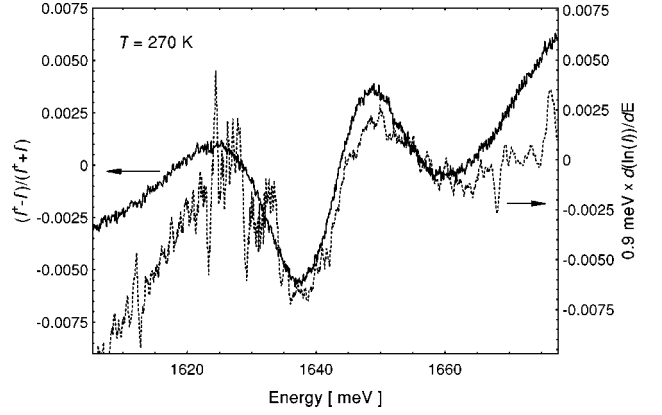


FIG. 4. Example comparison of circular polarization dichroism $(I_+ - I_-)/(I_+ + I_-)$ spectra and the derivative of the logarithm of reflectivity $0.9 \text{ meV} \times d[\ln(I)]/dE$, used for determination of the Zeeman splitting.

$\chi = 0$. We have done calculations for the two extreme cases of $\chi = 0$ and $\chi = 0.5$. None of these profiles reproduce either the Zeeman splitting or experimental slope of the magnetization. Experimental data can be described using the exponential profile, or (with a slightly smaller precision) using the ERF profile, whereas neither of the tested steplike profiles provide an acceptable description.

V. ZEEMAN EFFECT AT HIGH TEMPERATURE

The typical high-temperature spectra are presented in Fig. 4. Since the difference between the spectra measured in different circular polarization is small (even much smaller than the exciton linewidth) we chose to determine the Zeeman splitting from a comparison of the reflectivity spectrum $I(E)$ with the reflectivity polarization spectrum $(I_+ - I_-)/(I_+ + I_-)$ (cf. Ref. 17)

$$\frac{I_+ - I_-}{I_+ + I_-} = \frac{\Delta_{\text{Zeeman}}}{2} \frac{d}{dE} \ln(I). \quad (6)$$

The reflectivity feature related to the exciton ground state is well visible in both the reflectivity and reflectivity circular dichroism spectra. An example of the comparison between the dichroism spectra and a derivative of the logarithm of the reflectivity is presented in Fig. 4. The Zeeman splitting is determined by fitting the proportionality coefficient between

TABLE I. Values of intermixing length, coefficient β , and Zeeman splitting.

Sample	EXP intermixing l_{int} [Å]	$\alpha + \beta \times \ln(T/1 \text{ K}); \beta [10^{-5}]$ (Zeeman splitting at $B = 5 \text{ T}$ [meV])				Experiment
		EXP	ERF	Simulation		
				STEP ($\chi = 0$)	STEP ($\chi = 0.5$)	
SL 09124	4.65 ± 0.5	4.64 ± 0.19 (23.9)	4.81 (23.9)	1.88 (0.72)	3.06 (5.36)	4.19 ± 0.7 (23.9)
SL 09094	4.67 ± 0.5	5.66 ± 0.22 (21.2)	6.44 (21.2)	3.21 (0.39)	4.37 (2.88)	6.26 ± 0.7 (21.2)
SL 09074	4.88 ± 0.5	7.19 ± 0.26 (19.8)	7.86 (19.8)	4.95 (0.26)	6.00 (2.15)	7.22 ± 0.7 (19.8)

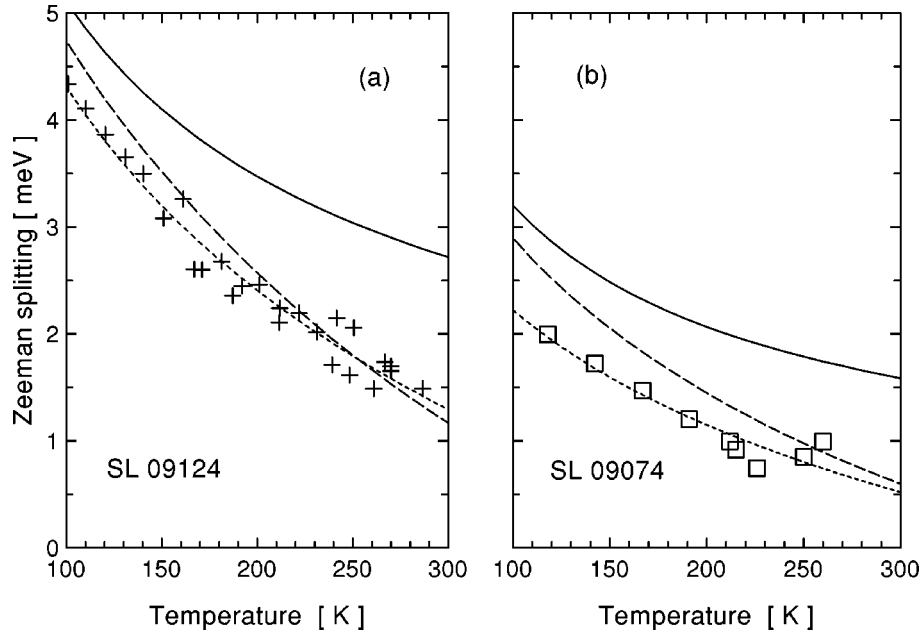


FIG. 5. The Zeeman splitting versus the temperature. Points represent experimental data; the solid line is calculated with superlattice parameters obtained from low-temperature Zeeman effect; the dashed line is obtained assuming a decrease of effective Zeeman effect due to thermal fluctuations; the dotted line is a guide for the eye.

the two curves, as indicated by Eq. (6). The accuracy of the method was checked by a test measurement performed for one of the superlattices (SL 09124) at a low temperature (1.9 K) in a very low-magnetic field. Under such conditions the splitting is proportional to the field and gives a precise test of the experimental procedure by comparison with a higher field splitting obtained directly from σ^+ and σ^- spectra. The error was less than 0.07 meV for the splitting of 2.44 meV. The Zeeman splitting versus temperature for both superlattices is presented in Figs. 5(a) and 5(b). The same figures show results of numerical calculation for high temperatures. The superlattice parameters were obtained from low-temperature data and then were used for simulations at higher temperatures. In the high-temperature region the exciton splitting was calculated using the same model as that developed for low temperatures. The potentials for electrons and heavy holes were calculated with the subband splitting obtained from the local magnetization in the particular positions in the structure. The splitting is given by the carrier-ion exchange constants $N_0\alpha=0.22$ eV and $N_0\beta=-0.88$ eV (Ref. 21)

$$\Delta V_{el}=N_0\alpha\langle S^z \rangle \quad \text{and} \quad \Delta V_{hh}=N_0\beta\langle S^z \rangle, \quad (7)$$

where $\langle S^z \rangle$ denotes the average spin per cation and is related to the local magnetization.¹⁹ $\langle S^z \rangle$ was calculated using Eq. (3) for a high-temperature magnetization.

Figures 5(a) and 5(b) show discrepancies between the experimental data and a calculation based on low-temperature fits. The calculation gives significantly stronger splitting than the measured one. In order to fit the high-temperature points, the interface mixing length would have to be reduced at these temperatures by at least 1.6 Å.

One of the mechanisms that may suppress the Zeeman splitting due to the interaction of the carriers with Mn^{++} ions is the usual (direct) Zeeman effect. In order to examine this possibility, one has to analyze nonmagnetic counterparts of CdTe/MnTe superlattices, e.g., CdTe/ $Cd_xZn_{1-x}Te$ CdTe/ $Cd_xMg_{1-x}Te$ superlattices. Measurements of such samples containing CdTe- $Cd_xZn_{1-x}Te$ heterostructures were reported for example in Ref. 22. Additionally, a pair of samples with the MnTe replaced by $Cd_xMg_{1-x}Te$ was tested by us. The average measured Zeeman effect at 5 T was 0.3 meV (never exceeded 0.5 meV). When the quantum wells are made of the same material (CdTe) and only the barriers are different ($Cd_{1-x}Mg_xTe$ or $Cd_{1-x}Mn_xTe$) the value of the nonmagnetic contribution to the Zeeman splitting should be similar. So the direct Zeeman effect is at least twice smaller than it would be necessary for explanation of the observed discrepancy.

As an explanation of the observed effect, we propose the exciton interaction with thermal fluctuations. Such interaction leads to the mixing of wave functions with zero and nonzero in-plane wave vectors.²⁴ Because of the complex structure of the valence band, the introduction of wave functions with $\mathbf{k}_{\parallel} \neq 0$ leads to a modification of selection rules, and thus changes the effective Zeeman splitting observed by modulation technique.

In order to understand the discussed effect we have to go beyond the simplest valence-band model (one dimensional), and analyze also wave functions with nonzero in-plane wave vectors $\mathbf{k}_{\parallel} \neq 0$. We make use of the numerical method presented in Ref. 23 with incorporated profiles of local Mn content and magnetization in direction perpendicular to the well plane, same as described above. The considered Hamiltonian is Luttinger and Bir-Pikus Hamiltonian, which in the basis of $|H\pm\rangle = 1/\sqrt{2}|3/2, +3/2\rangle_V \pm 1/\sqrt{2}|3/2, -3/2\rangle_V$, $|L\pm\rangle = 1/\sqrt{2}|3/2, -1/2\rangle_V \pm 1/\sqrt{2}|3/2, +1/2\rangle_V$ has the following form

$$H = \begin{pmatrix} |H+\rangle & |L+\rangle & |L-\rangle & |H-\rangle \\ P+Q & R'^- & 0 & 3B \\ R'^+ & P-Q & B & 0 \\ 0 & B & P-Q & R'^- \\ 3B & 0 & R'^+ & P+Q \end{pmatrix}. \quad (8)$$

If z direction is parallel to $[100]$ direction, the uniaxial approximation gives

$$P \pm Q = -\frac{\hbar^2}{m_0} \left[\frac{1}{2} (\gamma_1 \pm 2\gamma_2) k_z^2 + \frac{1}{2} (\gamma_1 \pm \gamma_2) k_{\parallel}^2 \right] + \frac{1}{2} [\beta_1 (2\varepsilon_{\parallel} + \varepsilon_{\perp}) \pm \beta_2 \varepsilon_{\parallel}],$$

$$R'^{\pm} = |R| \mp i|S|, \quad R = \frac{\sqrt{3}}{4} \frac{\hbar^2}{m_0} (\gamma_2 + \gamma_3) k_{\parallel}^2,$$

$$S = \frac{\hbar^2}{m_0} \sqrt{3} \gamma_3 k_{\parallel} k_{\perp}, \quad (9)$$

where in-plane and perpendicular components of strain tensor (ε_{\parallel} and ε_{\perp}) are given by the material lattice constants and elastic stiffness constants C_{ij}

$$\varepsilon_{\parallel} = [a(\text{CdTe}) - a(\text{Cd}_x\text{Mn}_{1-x}\text{Te})]/a(\text{CdTe}),$$

$$\varepsilon_{\perp} = -(2C_{12}/C_{11})\varepsilon_{\parallel} \quad (10)$$

and $\varepsilon_{\parallel\perp} = \varepsilon_{\parallel} - \varepsilon_{\perp}$. The antidiagonal elements B appear due to the exchange interaction with the localized Mn ions, and are given by local magnetization as it was discussed above

$$B = \frac{1}{6} N_0 \beta \langle S^z \rangle. \quad (11)$$

A typical result of calculations is presented on Fig. 6. For $k_{\parallel} = 0$ we get the same energies as for previous model and we obtain pure $|3/2, +3/2\rangle$, $|3/2, +1/2\rangle$, $|3/2, -1/2\rangle$, $|3/2, -3/2\rangle$ wave functions. For small values of in-plane wave

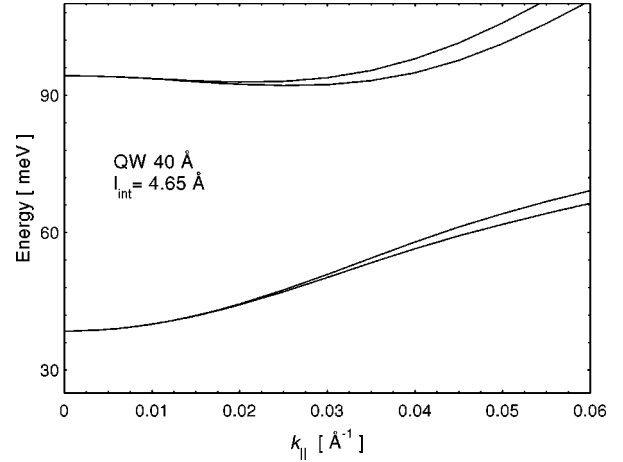


FIG. 6. Calculated dispersions of the lowest hole subbands in a 40 Å CdTe-MnTe quantum well.

vector the wave functions remains almost pure and subbands are parabolic. Significant nonparabolicity of the lowest heavy-hole subband appears above $k_{\parallel} = 0.02 \text{ \AA}^{-1}$. It is related to the mixing between pure wave functions. Admixture of wave functions with different spin momentum leads to a relaxation of the selection rules for optical transitions at high k_{\parallel} . Particularly in the Faraday configuration the transitions with both Zeeman-split hole subbands are allowed in each circular polarization. Thus, for narrow lines involving high k_{\parallel} we would expect to see two lines in the spectra taken for every circular polarization. If the linewidth is larger than the splitting (as in the case of the high-temperature measurements), the two lines could not be distinguished. If the modulation technique is applied for Zeeman effect measurements the obtained “splitting” is decreased by impure line polarizations. It can be shown that the modulation technique gives the distance between the average line energies in both polarizations ($Z = E_{\sigma^-} - E_{\sigma^+}$) weighted by the transitions probabilities. If neglecting the electron-hole exchange interaction the average line energies in both polarizations can be written in the following way

$$E_{\sigma^{\pm}} = \bar{\varepsilon} \frac{\sum_{i=1,2; m=\mp\frac{3}{2}, \mp\frac{1}{2}} m |\langle m|f_i\rangle|^2 [E_i + \Delta E_{\text{el}}(m \pm 1)]}{\sum_{i=1,2; m=\mp\frac{3}{2}, \mp\frac{1}{2}} |m| |\langle m|f_i\rangle|^2 + E_0}, \quad (12)$$

where $|f_1\rangle$ and $|f_2\rangle$ denote the wave functions of the two lowest hole levels (for $k_{\parallel} = 0$ they are just $|+3/2\rangle$ and $| -3/2\rangle$), E_1, E_2 denote their energies, and ΔE_{el} —splitting energy of the electron subband. The above formula takes much simpler form by noting that for splitting much smaller than the distance between ground and excited states, one can assume

$$|\langle +m|f_1\rangle|^2 = |\langle -m|f_2\rangle|^2. \quad (13)$$

The dominant terms in the k_{\parallel} dependence of Eq. (12) are those containing

$$(E_1 - E_2) (|\langle +3/2|f_1\rangle|^2 - |\langle +3/2|f_2\rangle|^2). \quad (14)$$

The effective “modulation technique” Zeeman splitting versus k_{\parallel} in relatively small magnetic field is presented on Fig. 7. The value of the splitting decreases significantly above $k_{\parallel} = 0.03 \text{ \AA}^{-1}$. The suppression of the Zeeman effect observed in high-temperature experiments is easily obtained for average $k_{\parallel} \approx 0.04 \text{ \AA}^{-1}$. In order to check the consistency of above calculations with low-temperature data one has to consider a free exciton. As long as the exciton remains delocalized there should be no important contributions of high

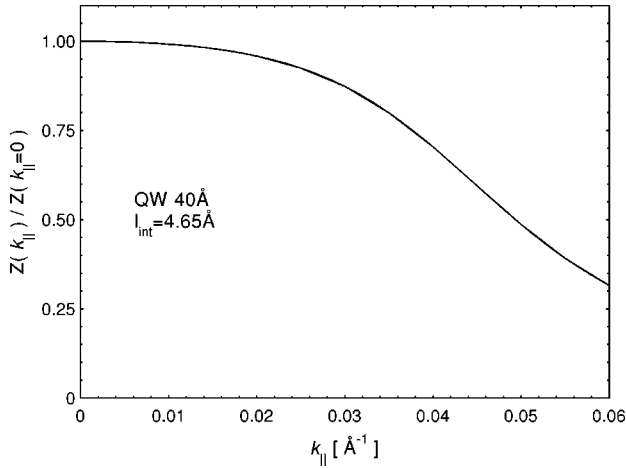


FIG. 7. An effective decrease of the Zeeman effect versus k_{\parallel} (calculated).

k_{\parallel} wave functions. The in-plane size of exciton in a quantum well is close to 100 \AA thus the exciton wave function is built of wave vectors smaller than k_{\parallel} for which bands become nonparabolic. This is the case of a low temperature: we observe splittings larger than the linewidth and within the experimental accuracy we see only one component at each circular polarization. Such a behavior is expected for transitions involving only states with negligible k_{\parallel} values. In a high-temperature thermal fluctuations may modify the wave function. It has been shown that interaction with thermal magnetic fluctuations results in the mixing between different \mathbf{k} states and leads to the modification of the energy gap.²⁴ The same effect in the case of a quantum well is much more difficult to handle quantitatively, since the magnetic fluctuation in inhomogeneous material has a more complex form, and may lead to the localization of the exciton. Nevertheless, the influence of the fluctuations on the exciton may be estimated from the temperature broadening of the exciton line. Unfortunately, the samples used for high-temperature Zeeman measurements are not suitable for line broadening analysis due to large inhomogeneous linewidth. Only in highest temperatures the significant temperature broadening may be observed. The linewidth reaches about 20 meV at 270 K. In order to avoid problems with experimental determination of thermal line broadening we use data of line broadening in other similar quantum wells.^{25,26} We assume average hole kinetic energy proportional to the line broadening, and use it for Zeeman effect calculation. If the full line width was 14 meV in 300 K,²⁶ we obtain reasonable agreement with observed decrease of the Zeeman splitting, by taking average kinetic energy equal to 0.75 of linewidth. The result of such approach is presented on Fig. 5 by dashed line. At low temperatures the mechanism we propose is not expected to introduce significant contribution to the measured Zeeman splitting. Within the second-order perturbation approximation used in Ref. 23, the contribution of the fluctuations is proportional to the product of temperature and magnetic susceptibility and therefore becomes insignificant at low temperatures. Experimentally, at low temperatures we are able to distinguish the Zeeman components and no significant relaxation of selection rules is observed, proving that influence of fluctuation is negligible.

In conclusion, we performed precise measurements of magnetic and magneto-optical properties of CdTe-MnTe superlattices up to the room temperature. The comparison of low-temperature exciton Zeeman effect to the measurements of magnetization performed by SQUID magnetometer shows a perfect agreement with used model, and allows to test manganese concentration profiles. Experimental data can be described using the exponential profile, or (with a slightly smaller precision) using the ERF profile, whereas neither of the tested steplike profiles provides an acceptable description. The analysis of the Zeeman splitting at high temperatures shows a decrease of exciton splitting with temperature faster than that deduced from Curie-Weiss law. We attribute that effect to the influence of thermal fluctuations on exciton states.

ACKNOWLEDGMENT

This work was partially supported by the Polish Committee for Scientific Research (Grants No. 2P03B01210 and No. PBZ 28.11).

APPENDIX

Calculation of magnetization for a MnTe/CdTe interface. In the local approximation the interface contribution to the magnetization in a superlattice consisting of CdTe wells of thickness a and MnTe barriers of thickness b reads

$$\chi_{\text{int}} = \frac{1}{a+b} \int_0^a \chi(z) dz.$$

Within the high-temperature expansion the susceptibility for any composition x of $\text{Cd}_x\text{Mn}_{1-x}\text{Te}$ mixed crystal obeys a Curie-Weiss law

$$\chi(x) = \frac{xC}{T-x\Theta},$$

where C and Θ are MnTe Curie constant and Curie-Weiss temperature, respectively. Assuming an exponential interface profile of width d $x(z) = \exp(-z/d)$ and noticing that $x(z)dz = -ddx$ we obtain

$$\chi_{\text{int}} = \frac{1}{a+b} \int_0^a \frac{x(z)C}{T-x(z)\Theta} dz = \frac{dC}{\Theta(a+b)} \int_{\exp(-a/d)}^1 \frac{dx}{T/\Theta - x}$$

and finally

$$\chi_{\text{int}} = \frac{dC}{\Theta(a+b)} \ln \frac{T-\Theta}{T-\Theta x(a)}.$$

Within the approximations $T \ll |\Theta|$ (rather crude) and $T \gg x(a)|\Theta|$ (quite well satisfied) we obtain the linear dependence of susceptibility on the logarithm of temperature. Since for not-too-thick barriers we can expect a not-too-strong temperature dependence for the barrier contribution, the above calculation holds approximately for the magnetization of the whole superlattice.

- ¹J.K. Furdyna, J. Appl. Phys. **64**, R29 (1988).
- ²W.C. Chou, A. Petrou, J. Warnock, and B.T. Jonker, Phys. Rev. Lett. **67**, 3820 (1991).
- ³N. Dai, H. Luo, F.C. Zhang, N. Samarth, M. Dobrowolska, and J.K. Furdyna, Phys. Rev. Lett. **67**, 3824 (1991).
- ⁴X. Liu, A. Petrou, J. Warnock, B.T. Jonker, G.A. Prinz, and J.J. Krebs, Phys. Rev. Lett. **63**, 2280 (1989).
- ⁵F.C. Zhang, N. Dai, H. Luo, N. Samarth, M. Dobrowolska, J.K. Furdyna, and L.R. Ram-Mohan, Phys. Rev. Lett. **68**, 3220 (1992).
- ⁶C. Benoit a la Guillaume, Yu. Semenov, and M. Combescot, Phys. Rev. B **51**, 14 124 (1995).
- ⁷D.R. Yakovlev and K.V. Kavokin, Comments Condens. Matter Phys. **18**, 51 (1996).
- ⁸A. Haury, A. Wasiela, A. Arnoult, J. Cibert, S. Tatarenko, T. Dietl, and Y. Merle d'Aubigné, Phys. Rev. Lett. **79**, 511 (1997).
- ⁹P. Kossacki, Nguyen The Khoi, A. Stachow, J.A. Gaj, G. Karczewski, J. Kossut, and T. Wojtowicz, Nuovo Cimento C **17**, 1537 (1995).
- ¹⁰J.A. Gaj, W. Grieshaber, C. Bodin-Deshayes, J. Cibert, G. Feuillet, Y. Merle d'Aubigné, and A. Wasiela, Phys. Rev. B **50**, 5512 (1994).
- ¹¹W. Grieshaber, A. Haury, J. Cibert, Y. Merle d'Aubigné, A. Wasiela, and J.A. Gaj, Phys. Rev. B **53**, 4891 (1996).
- ¹²P. Kossacki, Nguyen The Khoi, J.A. Gaj, G. Karczewski, T. Wojtowicz, J. Kossut, and K.V. Rao, Solid State Commun. **94**, 439-443 (1995).
- ¹³S. Kuroda, K. Kojima, K. Takita, K. Uchida, and N. Miura, *Proceedings of the International Conference on II-VI Compounds, Grenoble, 1997* [J. Cryst. Growth **184/185**, 971 (1998)].
- ¹⁴G. Wypiór, S. Kaiser, P. Kossacki, Nguyen The Khoi, J.A. Gaj, W. Gebhardt, G. Karczewski, T. Wojtowicz, and J. Kossut, Semicond. Sci. Technol. **13**, 93 (1998).
- ¹⁵A. Twardowski, H.J.M. Swagten, W.J.M. de Jonge, and M. Demianiuk, Phys. Rev. B **36**, 7013 (1987).
- ¹⁶T. Stirner, P. Harrison, W.E. Hagston, and J.P. Goodwin, Surf. Sci. **313**, 417 (1994); T. Stirner, W.E. Hagston, and P. Harrison, Phys. Rev. B **52**, R5519 (1995).
- ¹⁷D. Coquillat, J.P. Lascaray, J.A. Gaj, J. Deportes, and J.K. Furdyna, Phys. Rev. B **39**, 10 088 (1989).
- ¹⁸C. Testelin, C. Rigaux, and J. Cibert, Phys. Rev. B **55**, 2360 (1997).
- ¹⁹J. Kossut and W. Dobrowolski, *Diluted Magnetic Semiconductors, Handbook of Magnetic Materials*, edited by K.H.J. Bushow (Elsevier Science Publishers, New York, 1993), pp. 231–303.
- ²⁰J. Spałek, A. Lewicki, Z. Tarnawski, J.K. Furdyna, R.R. Gałazka, and Z. Obuszko, Phys. Rev. B **33**, 3407 (1986).
- ²¹J.A. Gaj, R. Planel, and G. Fishman, Solid State Commun. **29**, 435 (1979).
- ²²W. Grieshaber, C. Bodin, J. Cibert, A. Wasiela, Y. Merle d'Aubigné, J. Gaj, and G. Feuillet, in *Compound Semiconductor Epitaxy*, edited by C.W. Tu, L.A. Kolodziejski, and V.R. McCrary, MRS Symposia Proceedings No. 340 (Materials Research Society, Pittsburgh, 1994), p. 587.
- ²³G. Fishman, Phys. Rev. B **52**, 11 132 (1995).
- ²⁴R.B. Bylsma, W.M. Becker, J. Kossut, and U. Dębska, Phys. Rev. B **33**, 8207 (1986); J.A. Gaj and A. Golnik, Acta Phys. Pol. A **71**, 197 (1987).
- ²⁵N.T. Pelekanos, H. Haas, N. Magnea, H. Mariette, and A. Wasiela, Appl. Phys. Lett. **61**, 3154 (1992).
- ²⁶M. O'Neill, M. Oestreich, W.W. Ruhle, and D.E. Ashenford, Phys. Rev. B **48**, 8980 (1993).